Moroccan Journal of Chemistry
ISSN: 2351-812X
http://revues.imist.ma/?journal=morjchem&page=login
Tabti & al. / Mor. J. Chem. 10 N°4 (2022) 703-725
DOI: https://doi.org/10.48317/IMIST.PRSM/morjchem-v10i4.34319

CoMFA Topomer, CoMFA, CoMSIA, HQSAR, docking molecular, dynamique study and ADMET study on phenyloxylpropyl isoxazole derivatives for coxsackie virus B3 virus inhibitors activity

Kamal Tabti[(a)*], Larbi El Mchichi[(a)], Youness Moukhliss[(a)], Gagandeep Singh[(c,d)], Abdelouahid Sbai[(a)*], Hamid maghat[(a)], Mohammed bouachrine[(a,b)] and Tahar Lakhlifi[(a)]

[(a)] Molecular Chemistry and Natural Substances Laboratory, Faculty of Science, Moulay Ismail University of Meknes, Morocco

[(b)] EST Khenifra, Sultan Moulay Sliman University, Benimellal, Morocco.

[(c)] Section of Microbiology, Central Ayurveda Research Institute, Jhansi, Uttar Pradesh (284003), India

[(d)] Kusuma School of Biological Sciences, Indian Institute of Technology, Delhi, New Delhi (110016), India

** Corresponding author:*
a.sbai@umi.ac.ma
k.tabti@edu.umi.ac.ma
Received 18 Aug 2022,
Revised 02 Sept 2022,
Accepted 05 Sept 2022.

Abstract

Absent of drugs to treat entervirus infections, notably the coxsackievirus B3 virus (CVB3) which causes acute and chronic illnesses, the world remains in need of new antiviral drugs. The main objective of this work is the quantitative analysis of the structure-activity relationship (QSAR) of a series of phenyloxy propy isoxazoles derivatives against the CVB3 virus using two 2D approaches using the HQSAR method and 3D using the Topomer CoMFA and CoMFA and CoMSIA methods, followed by molecular docking analysis to validate established patterns and understand the mechanism of receptor-ligand interaction. The results of the 2D / 3D QSAR models are quite satisfactory and give significant statistical results: R^2 = 0.953, Q^2 = 0.819, R^2_{ext} = 0.750 for the HQSAR, R^2 = 0.980, Q^2 = 0.83, R^2_{ext} = 0.749 for the CoMFA topomer, R^2 = 0.977, Q^2 = 0.748, R^2_{ext} = 0.843 for CoMFA, R^2 = 0.962, Q^2 = 0.804, R^2_{ext} = 0.953 for CoMSIA. It can be noted that these four models exceeded the external validation criteria used with success and respected the limits of the criteria of Tropsha and Glorbaikh. Based on the results obtained from the four models, we proposed a candidate for each model as an inhibitory agent against CVB3. Docking analyzes and molecular simulation were performed to understand the mechanism of interactions of these four designed compounds within the receptor active site. small-sized electron donor groups molecular docking shows that the proposed compounds performed greater interactions than the more active compound in the database. However, the groups added for the molecules A1, A2, A3, A4 help to create additional interactions between these ligands and the residues to stabilize the conformation of the ligands at the level of the binding pocket. The stability and binding modes of compounds A1, A2 and the most active compound in the data set were evaluated by molecular dynamics simulations during a simulation time of 100 ns. It is shown that the interactions of the selected compounds are stable and fluctuate weakly in the complex. Free energy calculations based on the MM-GBSA method confirmed that the two designed compounds A1 and A2 were able to form bonds in the protein cavity. In addition, the ADMET study and the five-parameter Lipinski's rule prediction were estimated to ensure that the proposed candidates are viable drugs with synthetic accessibility. These results can be used for the discovery of new drugs and can solve the problem of resistance of the CVB3 virus

Keywords: *Coxsackie virus B3, phenyloxylpropyl isoxazole, CoMFA topomer, HQSAR, CoMFA, CoMSIA, Docking molecular, MD simulation, MMGBSA.*

1. Introduction

Coxsackievirus B3 (CVB3) is a member of the enterovirus genus of the picornavirus family [1]. Numerous research have demonstrated that these types of viruses can produce a wide spectrum of acute and chronic diseases, including mild respiratory infections, foot-and-mouth disease[2]. Including mild respiratory infections, foot-and-mouth disease, herpangina, hemorrhagic conjunctivitis, pleurodynia, and life-threatening gastrointestinal diseases such as myocarditis[3], aseptic meningitis[4], brainstem encephalitis, and septic syndrome in neonates[5]. In addition, epidemiological data show that Coxackie viruses may be involved in the pathogenesis of type 15 diabetes. To date, these viral infections are treated symptomatically. As there are about 65 serotypes of human enter viruses. There are no effective vaccines against enter viruses and, to date, there are no antiviral agents available to treat life-threatening infections. Therefore, it has become urgent to find new effective drugs against enteroviruses that could remedy this unacceptable situation [6,7]. In searching for anti-CVB3 agents, a new class of compounds, derived from phenyloxy propyl isoxazole, and we focused our attention on the effect of different substitutions of the purine moiety on the antiviral activity against CVB3 virus. In the present study, a structure-activity relationship was generated by QSAR method in two and three dimensions, to explain and justify the activity against CVB3 of phenyloxy propyl isoxazole, in order to propose promising drugs[8-10]. To do so, we have to rely on four methods: CoMFA topomer, CoMFA, CoMSIA and HQSAR. The results of the four models were used as a guide for the design of four new molecules of high activity against the CVB3 virus. The viability of these new candidates and their bioavailabilities were ensured by the ADMET study[11]. Molecular docking studies and MD simulations for 100 ns were achieved to understand the binding modes and stability of ligand-receptor complex interactions[12,13]. Binding free energy computations by MolecularMechanics/Generalized Born Surface Area method were performed to confirm binding affinities and to explore the interactions that regulate the binding of inhibitors to CVB3 virus.

2. Materials and methods

1.1. ***QSAR modeling database and optimization***

In this study, a data set of 49 of phenyloxylpropyl isoxazole derivatives , which have been studied as antiviral agents against the coxsackie virus B3 virus were reported from the literature[14-17]. The IC_{50} values determined against CVB3 97-927 in HeLa cells are in µg / ml were transformed to pIC_{50} (M) [$pIC_{50} = -\log_{10}(IC_{50}.)$] Table 1. The molecular structures of all compounds in the dataset were designed and optimized through a SYBYL-X 2.0 program using the Powell gradient, with 0.05kcal/mol. A in convergence criterion method by Tripos force field and Gasteiger-Huckel charges with 10,000 iterations[18].

Table 1. ***Database with the experimental pIC_{50} values and that predicted by the 2D and 3D-QSAR models***

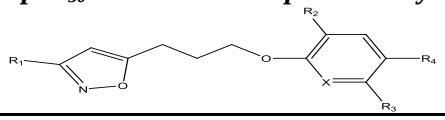

N°	R_1	R_2	R_4	R_3	X	pIC_{50}	CoMFA		CoMSIA		CoMFA topomer		HQSAR	
							Pred	Residu	Pred	Residu	Pred	Residu	Pred	Residu
1	CH_3	CH_3	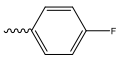	H	CCH_3	5.404	5.170	-0.234	5.057	-0.347	4.83	-0.574	5.087	-0.317
2	CH_3	CH_3	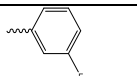	H	CCH_3	4.951	5.127	0.176	5.019	0.068	4.85	-0.101	5.125	0.174
3	CH_3	CH_3	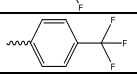	H	CCH_3	4.510	4.360	-0.15	4.586	0.076	3.84	-0.67	4.752	0.242
4	CH_3	CH_3	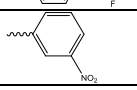	H	CCH_3	4.779	4.641	-0.138	4.713	-0.066	4.28	-0.499	4.805	0.026
5	CH_3	CH_3	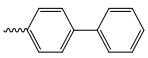	H	CCH_3	3.865	3.891	0.026	3.802	-0.063	3.51	-0.355	3.673	-0.192
6	CH_3	CH_3	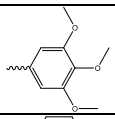	H	CCH_3	4.619	4.785	0.166	4.821	0.202	4.11	-0.509	4.518	-0.101
7	CH_3	CH_3	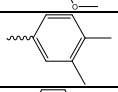	H	CCH_3	5.149	4.961	-0.188	4.461	-0.688	3.94	-1.209	4.669	-0.48
8	CH_3	CH_3		H	CCH_3	4.511	4.455	-0.056	4.793	0.282	4.19	-0.321	4.466	-0.045
9	CH_3	CH_3	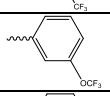	H	CCH_3	4.574	4.512	-0.062	4.714	0.14	4.47	-0.104	4.586	0.012
10	CH_3	CH_3		H	CCH_3	5.275	5.197	-0.078	5.160	-0.115	4.94	-0.335	4.646	-0.629
11	CH_3	CH_3	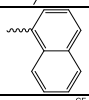	H	CCH_3	4.979	4.720	-0.259	4.579	-0.4	4.59	-0.389	5.126	0.147
12	CH_3	CH_3	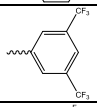	H	CCH_3	3.961	3.720	-0.241	3.978	0.017	3.52	-0.441	3.711	-0.25
13	CH_3	CH_3	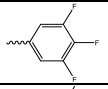	H	CCH_3	5.000	4.997	-0.003	4.857	-0.143	5.00	0	4.989	-0.011
14	CH_3	CH_3	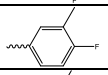	H	CCH_3	4.270	4.752	0.482	4.769	0.499	4.42	0.15	4.813	0.543
15	CH_3	CH_3		H	CCH_3	3.840	3.913	0.073	4.279	0.439	4.06	0.22	4.385	0.545
16	CH_3	CH_3	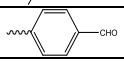	H	CCH_3	4.540	4.576	0.036	4.717	0.177	3.76	-0.78	4.440	-0.1
17	CH_3	CH_3	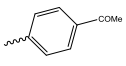	H	CCH_3	3.86	4.154	0.294	3.854	-0.006	3.30	-0.56	4.296	0.436
18*	CH_3	CH_3	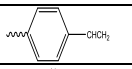	H	CCH_3	3.240	4.701	1.461	4.658	1.418	4.09	0.85	4.363	1.123
19	CH_3	CH_3	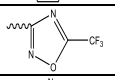	H	CCH_3	7.470	7.713	0.243	7.874	0.404	7.91	0.44	7.863	0.393
20*	CH_3	H	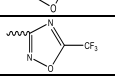	H	H	5.990	6.926	0.936	7.487	1.497	7.08	1.09	7.753	1.763
21	CH_3	CH_3	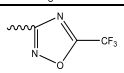	H	H	8.292	8.158	-0.134	8.054	-0.238	7.95	-0.342	7.873	-0.419
22	CH_3	OCH_3	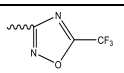	H	H	7.39	7.428	0.038	7.196	-0.194	7.33	-0.06	7.515	0.125
23	CH_3	Br	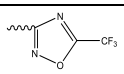	H	H	8.64	8.504	-0.136	8.506	-0.134	8.29	-0.35	8.761	0.121

24	COOMe	CH_3	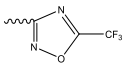	H	CCH_3	7.221	6.863	-0.358	6.942	-0.279	7.10	-0.121	6.978	-0.243
25	COOEt	CH_3	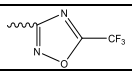	H	CCH_3	7.155	7.221	0.066	7.233	0.078	6.80	-0.355	6.802	-0.353
26	COOIsopro	CH_3	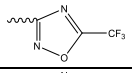	H	CCH_3	6.721	6.750	0.029	6.677	-0.044	6.54	-0.181	6.721	0
27	Ph	CH_3	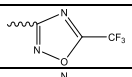	H	CCH_3	6.854	7.183	0.329	6.894	0.04	6.73	-0.124	6.915	0.061
28*	NH_2	CH_3	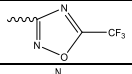	H	CCH_3	7.155	7.972	0.817	8.024	0.869	7.37	0.215	7.13	-0.025
29	MeNH	CH_3	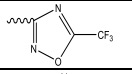	H	CCH_3	7.221	7.425	0.204	7.496	0.275	6.90	-0.321	6.997	-0.224
30*	$PhCH_2NH$	CH_3	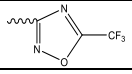	H	CCH_3	5.857	6.692	0.835	6.765	0.908	6.64	0.783	6.427	0.57
31	MeNH	CH_3	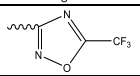	H	CCH_3	7.699	7.563	-0.136	7.418	-0.281	7.62	-0.079	8.016	-1.272
32	COOEt	H	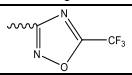	H	CH	6.127	6.373	0.246	6.365	0.238	5.97	-0.157	6.541	1.889
33	COOEt	H	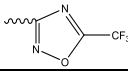	H	COMe	6.31	6.628	0.318	6.276	-0.034	6.21	-0.1	6.234	0.231
34	COOEt	H	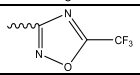	H	CF	6.664	6.571	-0.093	6.726	0.062	6.95	0.286	6.697	-0.43
35	COOEt	H	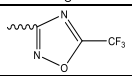	H	CCF_3	7.523	7.388	-0.135	7.397	-0.126	7.44	-0.083	7.472	-0.826
36	COOEt	MeO	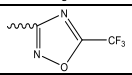	H	CNO_2	5.925	5.789	-0.136	5.983	0.058	5.60	-0.325	5.662	1.547
37	$CONMe_2$	H	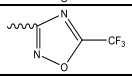	H	H	6.339	6.685	0.346	7.001	0.662	6.79	0.451	6.449	-0.677
38	$CONMe_2$	H	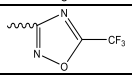	H	COMe	7.523	7.506	-0.017	6.823	-0.7	7.04	-0.483	7.405	-1.074
39	$CONMe_2$	H	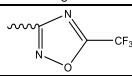	H	CNO_2	8.523	8.220	-0.303	8.426	-0.097	8.38	-0.143	8.209	-1.118
40*	$CONMe_2$	H	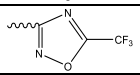	H	CCF_3	6.796	7.961	1.165	8.046	1.25	8.27	1.474	8.643	1.413
41	$CONMe_2$	OMe	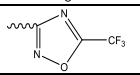	H	CNO_2	6.437	6.796	0.359	6.504	0.067	6.42	-0.017	6.832	2.206
42	CONHMe	H	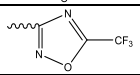	H	CCF_3	7.699	7.717	0.018	8.100	0.401	7.55	-0.149	7.624	-0.867
43*	COOEt	NH_2	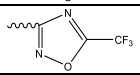	H	H	4.699	4.756	0.057	5.398	0.699	6.56	1.861	5.611	2.925
44	CONHMe	CH_3	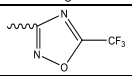	H	CCH_3	4.991	4.768	-0.223	4.642	-0.349	5.02	0.029	4.996	0.62
45	COEtNH	CH_3	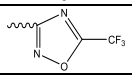	H	CCH_3	4.700	4.712	0.012	4.912	0.212	4.35	-0.35	4.874	0.296
46*	$CONMe_2$	H	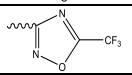	H	CNH_2	5.350	7.229	1.879	6.434	1.084	7.39	2.04	6.782	-0.476
47*	$CONMe_2$	H	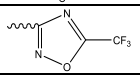	H	NHCOMe	4.521	5.410	0.889	5.689	1.168	6.45	1.929	6.329	2.261
48	$CONMe_2$	H	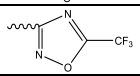	H	pyrrolyl	6.086	6.029	-0.057	6.244	0.158	5.85	-0.236	6.167	0.243
49	$CONMe_2$	H	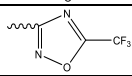	H	NH	7.84	7.516	-0.324	7.591	-0.249	7.63	-0.21	7.748	-1.673

*1.2. **Generality of CoMFA and CoMSIA analysis***

The CoMFA and CoMSIA analyzes are 3D methods QSAR consists of putting a quantitative relationship to explain a dependent variable (pIC_{50}) by calculating 3D descriptors such as steric (S) electrostatic (E), hydrogen bond donor (HBD), and acceptor hydrogen bond (HBA)[19]. In the CoMFA analysis, steric and electrostatic fields were determined; where the generated energy fields were calculated at each pattern of the lattice based on the Lenard-Jones potential and the Columbia potential to calculate the electrostatic and steric factors respectively, the values of potential used is set around 30.0 kcal/mol. For the CoMSIA analysis is based on a grid that included steric, electrostatic, hydrophobic fields H-Bond Donor H-Bond Acceptor. All these factors were determined at each lattice point of the grid box using a probe atom with a radius of 1 Å and charge + 1 for the five fields. Molecular atoms and those probed for all points of the grid a was determined using the Gaussian function. Molecular alignment is a curcial step in 3D-QSAR, directs the orientation of molecules in 3D space[20]. Several alignment techniques presented in SYBYL-X2.0, in this work the rigid distill technique was used because it showed important results in several studies [21]. all compounds were aligned with the most active compound N°23 as a template [22] (Figure.1).

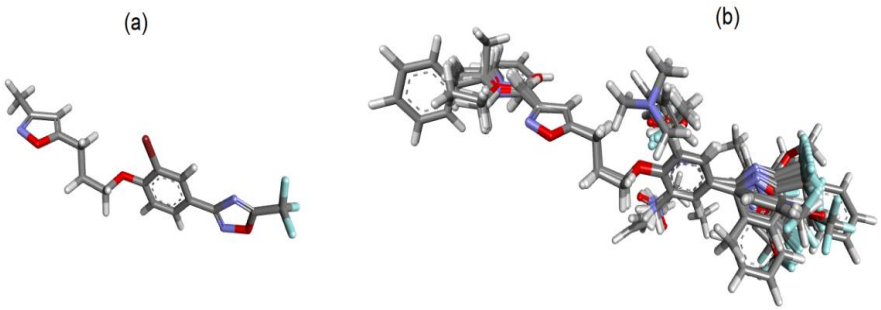

Figure 1. (a) 3D-QSAR structure superposition of training set (b) compound N°23 as a template

1.3. ***HQSAR analysis***

Hologram QSAR (HQSAR) is a two-dimensional QSAR method, which links biological activities to molecular structure in terms of sub-structural fragments. This method avoids complexations associated with 3D-QSAR methods, such as three-dimensional structure alignment and putative binding conformation[23]. In addition, this method does not require determining and calculating the Physico-Chemical descriptors relating to the classic QSAR, which takes a lot of time. In this method, each molecule in the dataset is divided into several non-structural fragments, which are arranged to form a molecular hologram[24]. The length of the (HL) is set by default to the values (53, 59, 61, 71, 83, 97, 151, 199, 257, 307, 353, and 401). The molecular substructure of the dataset is defined from 4 to 7 and represents the fragments size, and the fragment distinction used are atoms (A), bonds (B), connections (C), hydrogen atoms (H), chirality (Ch), and donor and acceptor (DA) [25].

1.4. ***Topomer CoMFA analysis***

The CoMFA topomer method has been realized to transcend the alignment limitation in CoMFA, this technique takes into account not only the steric and electrostatic descriptors but also the molecular topomer descriptors [26]. A topomer is defined as a molecular fragment with a single internal geometry or "Pose". The two main fragmentation techniques (R_a – R_b and R_a- Common-Core-R_b) were performed to generate better models (Figure.2). The calculation of steric and electrostatic fields is similar to the CoMFA method [27].

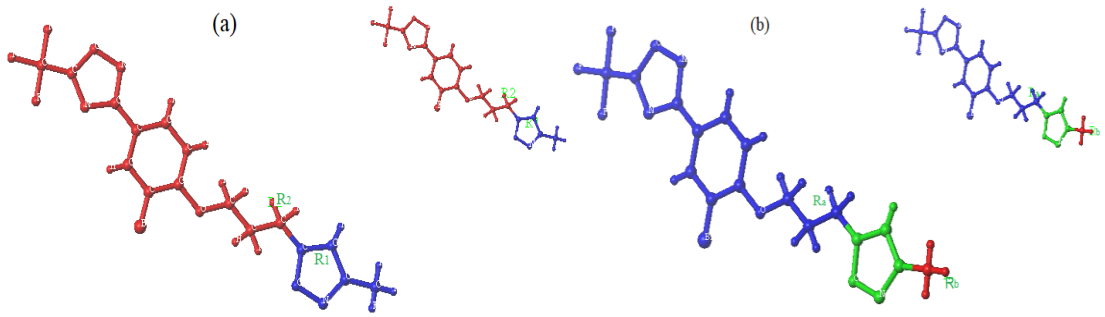

Figure 2. Cutting mode in CoMFA topomer (a) Ra – Rb and (b) Ra-Common Core-Rb

*1.5. **Protocol to build and validate models***

3D / 2D-QSAR models were derived using the PLS regression algorithm. This method has proven to be very effective in numerous studies for evaluating the relationships between the different molecular composition descriptors and the pIC_{50} activity values of the compounds studied using this method [28]. The internal validation of the models was carried out by the LOO method by calculating the coefficient Q^2 (no validation) to estimate the robustness and the predictive capacity of the models built [29]. The optimal number of compounds in the models was determined for high values of Q^2. The models were generated for small values of SEE using the correlation coefficient R_2. Whereas the predictive power of the models was estimated by the R^2_{pred} of the test set. While the predictive power of the models was estimated by the R^2_{pred} of the test set.

$$Q^2 = 1 - \frac{\Sigma(Y_{exp} - Y_{pred})^2}{\Sigma(Y_{expe} - Y_{mean})^2}; \quad SEE = \sqrt{\frac{\Sigma_{i=1}^{n} Y_{exp} - Y_{pred})}{n-2}}$$

Much research in the literature has been shown that a high value of q^2 is a necessary but insufficient condition for judging the reliability of models[30]. For this work, criteria of Golbraikh-Tropsha and statistical metrics of Roy were reported to meet these needs and are defined by the following equations[31]:

- $r_0^2 = 1 - \frac{\Sigma(Y_{exp} - k\,x\,Y_{pred})^2}{\Sigma(Y_{exp} - Y_{pred})^2}$
  - $k = \frac{\Sigma(Y_{exp}\,x\,Y_{pred})}{\Sigma(Y_{pred})^2}$
  - $\overline{r^2_m} = \frac{(r_m^2 + r'^2_m)}{2}$
- $r_m^2 = r^2(1 - \sqrt{|r^2 - r_0^2|}$

- $r_0'^2 = 1 - \frac{\Sigma(Y_{Pred} - k' x\,Y_{exp})^2}{\Sigma(Y_{Pred} - Y_{exp})^2}$
  - $k' = \frac{\Sigma(Y_{exp}\,x\,Y_{pred})}{\Sigma(Y_{exp})^2}$
  - $\Delta r_m^2 = |r_m^2 - r'^2_m|$

We assume an acceptable QSAR model if:

The value of " r02, r'0^2, $\bar{}$r²m, rm^2 and rm'² must be > 0.5, (r² - r²0) /r² , (r² - r'²0) /r² should be < 0.1, $\Delta r2m$ must be < 0.2, and k and k' must be between 0.85 and 1.15 [32].

*1.6. **Docking molecular Simulation***

Molecular docking was performed on the one hand to validate the contour maps of the QSAR models and on the other hand to understand the mechanism of the bonding reaction of the active site, using Autodock 1.5.6 software. In this present work, we anchored the most active compound in the chain from our database, with the protein (PDB ID: 3ZZD) being extracted from the RCSB protein database and modified for anchoring calculations [33,34]. In the first step of molecular docking, water molecules were extracted from the crystal structure, and then polar hydrogen atoms were added to the protein skeleton by linking protein side chains. The final step of protein preparation is that the

Gasteiger-Huckel charge is mapped to each protein atom [35]. The docking was carried out by docking the ligand in the active site occupied by the legand father G85. Nine modes were created. To choose the appropriate mode, we base ourselves on the lower value of the affinity.

1.7. ***MD Simulations***

The system for MD was prepared using LiGRO tool usig GROMACS 5.1.5. The Amber99sb forcefield was used for protein, the topology for ligands was generated using ACPYPE module of LiGRO using GAFF (General Amber Force Field) for ligand with bcc charges, system was neutralised with 0.15 M NaCl , system was energy minimized using 5000 steps of steepest descent followed by conjugate gradient. The NVT(modified berendson thermostat) , NPT (parinello-rehman barostat) equilibrium was done for 1ns each and production run for 100ns. All bonds were restrained using LINCS algorithm and electrostatic corrections using PME. The time step of 2fs and each frames were stored after every 10ps.

1.8. ***Post simulation binding free energy analysis***

MM-GBSA is a powerful technique for calculating binding free energy in the ligand-protein complex. In our research, the binding free energy of MM-GBSA was calculated using the package gmx_MMGBSA based on MMGBSA.py [36,37]. The free energy of protein-ligand binding of MM-GBSA can be given by the following equation:

$$\Delta G_{Bind} = \Delta G_{complex} - \Delta G_{protein} - \Delta G_{ligand}$$

where $\Delta G_{complex}$ designates the total free binding energy between the complexe. The total free energy of protein and ligand in the solvent was expressed as $\Delta G_{protein}$ and ΔG_{ligand} respectively.

3. Results and discussion

3.1. HQSAR statistical results

In this study to generate the HQSAR models we made numerous combinations of fragments distinction including atomic number (A), bond type (B), atomic connection (C), chirality (Ch), hydrogen (H) and hydrogen bond donor / acceptor (DA) with a fragment size 4 -7. The results of best ten models generated are summarized in Table 2. We could notice that each change in fragment distinction reflects a change in the pIC_{50} value, which shows the direct correlation of fragment and biological activity. The results suggest that the atomic number (A), the type of bond (B), atomic connection (C), chirality (Ch), and hydrogen bond donor / acceptor (DA) are involved in the construction of the best model, and shows values of R^2 and Q^2, of order of 0.789 and 0.956 respectively, the optimal number of components ONC is 5.

Table 2. ***Statistical results of HQSAR including different fragment distinction***

Fragment distinction	Q^2_{LOO}	R^2	SEE	Best LH	ONC
A	0.726	0.900	0.496	151	6
B	0.612	0.882	0.537	307	6
C	0.749	0.920	0.442	199	6
H	0.677	0.771	0.728	97	4
Ch	0.677	0.771	0.728	97	4
DA	0.715	0.896	0.498	353	5
A/B/C/Ch/DA	0.798	0.956	0.328	199	5
A/B/C/H/CH/DA	0.738	0.905	0.469	353	4

Table 3. ***Statistical results of HQSAR including different fragment sizes***

Fragment distinction	Fragment size	Q^2_{LOO}	R^2	SEE	Best LH	ONC
A/B/C/Ch/DA	1 - 4	0.721	0.906	0.467	307	4
A/B/C/Ch/DA	2 - 5	0.714	0.926	0.427	97	6
A/B/C/Ch/DA	3 - 6	0.764	0.938	0.389	97	6
A/B/C/Ch/DA	4 - 7	0.798	0.956	0.328	199	6
A/B/C/Ch/DA	5 - 8	0.789	0.953	0.338	97	6
A/B/C/Ch/DA	6 - 9	0.799	0.959	0.318	199	6
A/B/C/Ch/DA	7 -10	0.819	0.953	0.334	151	5
A/B/C/Ch/DA	8 – 11	0.804	0.964	0.311	199	6
A/B/C/Ch/DA	9 – 12	0.794	0.957	0.321	151	6
A/B/C/Ch/DA	10 – 13	0.750	0.962	0.307	151	6
A/B/C/Ch/DA	11 - 14	0.735	0.955	0.331	257	6
A/B/C/Ch/DA	12 - 15	0.712	0.900	0.423	257	6

Table 3 shows the results of the model selected by changing the fragment size. Which shows the influence of fragment size on the improvement of the statistical parameters of models, the best model selected with a fragment size is 7 - 10, the values of R^2 and Q^2 are respectively 0.953 and 0.819 and the values of best Hologram Length and ONC are 151 and 5 respectively.

3.2. CoMFA and CoMSIA resultats

In this current work, the CoMFA and CoMSIA models have been established to predict the predictive activity of pIC_{50} against CVB3 virus in terms of 3D descriptors. The CoMFA model explains the activity selected in terms of steric and electrostatic; and to determine the best CoMSIA models we performed several combinations of steric and hydrophobic electrostatic fields and hydrogen bond donor/acceptor. The statistical parameters of the models obtained are collected in Table 4. The CoMFA model shows statistically significant results with values of R^2, Q^2 is 0.977 and 0.748 respectively, and a value of ESS and F of order 0.239 and 238.083 respectively. The optimal number of component is acceptable compared to the size of the database of (ONC = 5). The CoMSIA / SHD model results reveal interesting values of R^2 and Q^2 of the order of 0.962 and 0.839. The values of F of ESS and ONC are 134.252, 0.315 and 5 respectively.

3.3. CoMFA topomer results

CoMFA Topomer is an interesting, near-fast QSAR patterning method for overcoming the alignment of compounds in the training and testing set. In this work, to find the best fragmentation of Topomer CoMFA model, two types of fragmentations were generated on the N°23 compounds as a reference. Ra-Rb fragmentation: the structure is divided into two parts by cutting the isoxazole and phenyloxy propyl bond (topomer CoMFA-1).

Ra- common core - Rb fragmentation: the structure is deviser in three parts, the bond which connects isoxazole and phenyloxypropyl to form Ra, the bond which connects methyl and isoxazole to form Rb and the common core is isoxazole (CoMFA topomer-1). Table 5 shows the statistical results of two generated topomer CoMFA models (topomer CoMFA-1) and (topomer CoMFA-2). Both models suggest good results with an advantage of CoMFA-1 model, with values of R^2 and Q^2 were respectively 0.980 and 0.830.

Table 4. ***Statistical indicators of the 3D QSAR models***

model		CoMFA : E+S	CoMSIA : S+ H+A	All : E+ S+H+ D+ A
R^2		0.977	0.962	0.943
Q^2		0.748	0.804	0.740
SEE		0.239	0.315	0.372
F		238.083	134.252	94.625
ONC		5	5	6
Fractions		0.648	0.307	0.177
		0.352	-	0.214
		-	0.311	0.205
		-	-	0.060
		-	0.382	0.344

Table 5. ***Results from two CoMFA topomer models studies***

	topomer CoMFA-1	topomer CoMFA-2
ONC	7	7
R^2	0.980	0.97
SEE	0.67	0.67
Q^2	0.83	0.82
intercept	7.3	7.1

3.4. Interpretation HQSAR contribution map

The QSAR model is graphically simplified by colored structures where the color of each atom reflects a positive or negative contribution on the activity of the compounds, so to visualize the contribution of the HQSAR map; the atoms (fragments) of more active and less active compounds have been shown with the collared spectrum in Figure 3. The colors ranging from yellow, yellow-green to green represented a favorable contribution to the values of pIC_{50}, while the colors red, red-orange and orange indicated an unfavorable contribution to the value of pIC_{50}. The white fragments represented an intermediate contribution to the values of pIC_{50}. These results show the fragments responsible for the biological activity and the fragments which could be modified to increase the activity. The evaluation of the contribution maps on the most active compound N°23 showed at the positive end of the spectrum, the oxadiazole group was covered by green color; thus the methyl of 2,4 -Diazafuranune group has been covered by yellow-green color. This showed the importance of these substituents to improve the biological activity Figure 3.

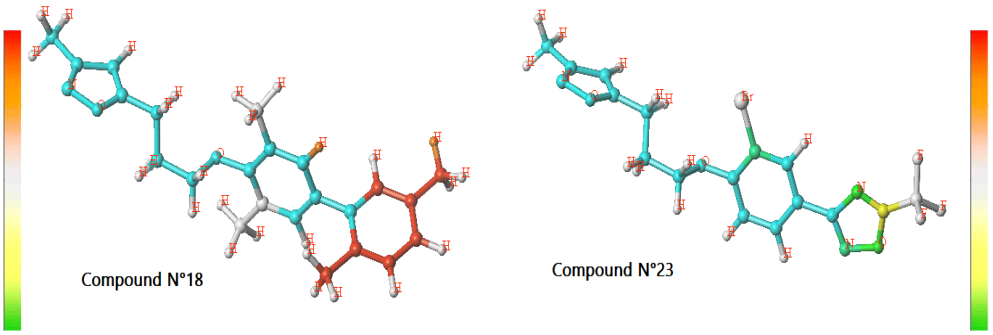

Figure 3. Residual plots between experimental and predicted values for HQSAR model.

Also the carbon atom linked to the Br group at position R2 has been covered by a green color, which signifies the importance of carbon at this position on the value of the activity. On the other hand, compound N°18 as the less active compound in the training set was located at the red end of the spectrum showing that the atoms of this compound decreased the activity. The dimethyl phenyl substitute at the R4 position in red indicates the negative influence of this group to biological activity.

3.5. Interpretation maps of 3D QSAR analysis

To visualize the results relating to the 3D QSAR models, and to identify the regions of the steric, electrostatic, hydrophobic, H-B Donor and H-B Acceptor field distributions, on the structure of compound N°23 (pIC50= 8.62) as a template, we used the maps of contours. The models resulting from the CoMFA, CoMSIA and Topomer CoMFA analysis were graphically translated by colored contour maps, where each colored contour shown reflected the desirable and undesirable contribution.

- **CoMFA contours maps**

In the case of CoMFA analysis, the steric map is represented by green and yellow contours, where the green and yellow outlines indicate a favorable and unfavorable contribution plus with the sterically bulky groupings respectively. Figure 4(a) represents four main green contours near Br of position R2), methyl of position R1, and near oxadiazole of position R4 and in particular around the nitrogen atom 1 and the methyl group of 2, 4-Diazafuran. These results indicate the need for large steric groups at these sites to enhance biological activity. Which explains the increase in activity if the hydrogen in position R2 (compound N°18; pIC_{50} = 5.00) is replaced by methyl (compound N°21 (pIC_{50} = 8.292). While two small yellow areas are in the vicinity of the binding carbon of phenyl and 2, 4-Diazafuran, less substituent groups at this position could increase activity.

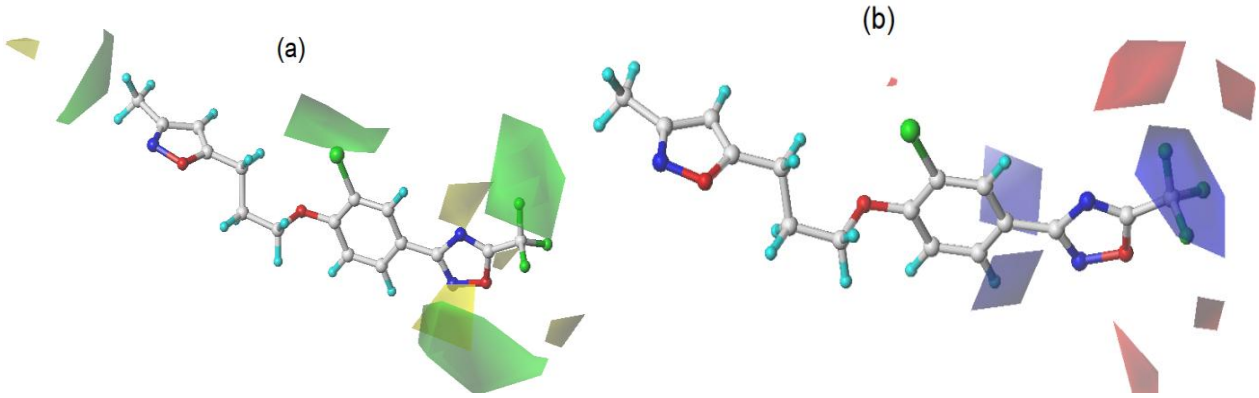

Figure 4. CoMFA contour maps analysis steric (a), Electro (b) on compound N°23

The electrostatic map is represented by red and blue colors, where the red and blue colors indicate an increase or decrease in biological activity respectively. Figure 4(b) shows blue and red outlines scattered over the molecule, but the closest and clear contour is found near the methyl group of oxadiazole at position 4, which meant that an electron donor group at this position could increase activity.

• CoMSIA contours maps

The best combination of fields obtained from the CoMSIA analysis is with a contribution of steric, hydrophobic and hydrogen binding acceptor fields (CoMSIA / SHA). The CoMSIA steric contour map is shown in Figure 5(a). This showed a steric contour similar to that of CoMFA but larger in size. Therefore, this result and confirms the steric contour maps in the CoMFA model. Figure 5(b) represents the hydrophobic contour map where the yellow and white

color represents a favorable (80%) and unfavorable (20%) contribution respectively. A yellow contour is observed near the R2 position, indicating a hydrophobic group in this position causing an improvement in the activity of the molecules. While the substitution of R1 and R4 is surrounded by white color, suggesting that a hydrophilic group at these positions could cause an increase in biological activity.

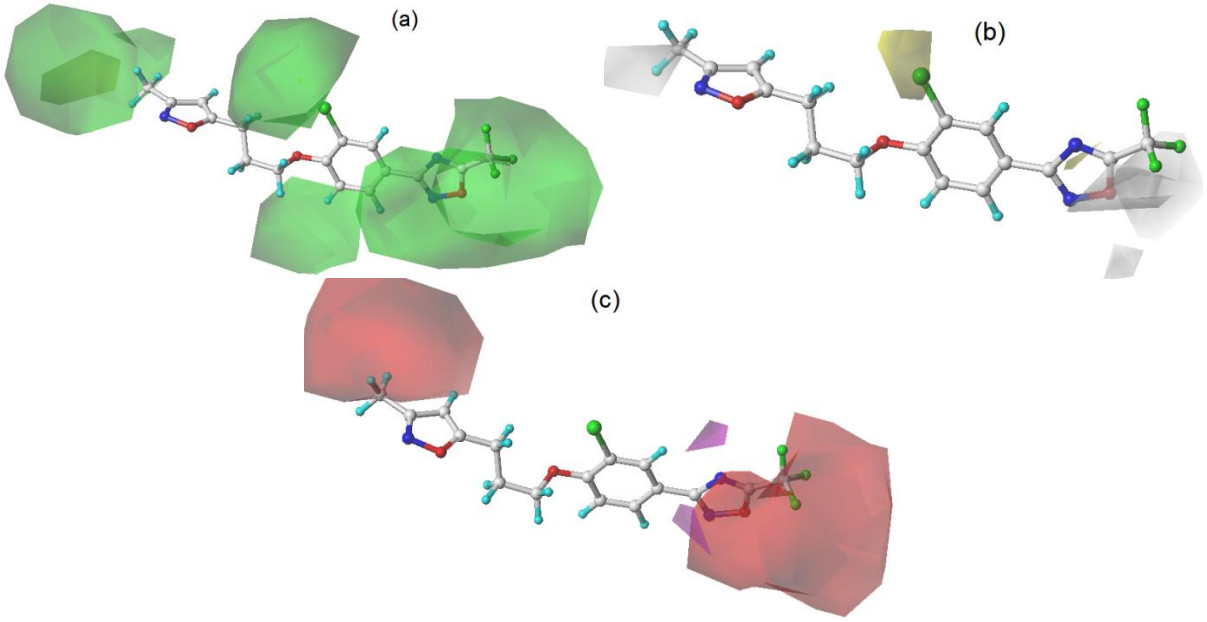

Figure 5. CoMSIA contour maps analysis steric (a), hydrophobic (b) and acceptor H-Bond (c) on compound N°23.

As shown in Figure 5(c) above, a red contour covered the methyl group at R_1 and at R_2. These results show that hydrogen bond acceptor substitutes in these positions can increase the biological activity. This result explains the decrease in the value of pIC_{50} decreased if by comparing the activity of compound N°19 (pIC_{50} = 7.47) and of compound N°25 (pIC_{50} = 7.155) where an acceptor group of the hydrogen bond is located in position R_1 associated with a month activity low.

• CoMFA topomer contour maps

The generation of the contour maps in the CoMFA topomer model is based on the Ra and Rb fragments, the CoMFA-1 topomer model shows is good predictive, Figure 6 represents the contour maps generated around fragment Ra (Figure 6(a) and Figure 6(b)) and around fragment Rb (Figure 6(c) and Figure 6(d)). Figure 6(a) represents the steric contour map of the R1 fragment, a green color surrounds the methyl at the R1 position, signified that this position is favorable by steric hinder group. While the steric contour map of the R2 fragment shown in Figure 6(c) shows a yellow color near the oxadiazole methyl and a green color near the Br atom at the R2 position; indicated the presence of steric bulky groups favorable and unfavorable respectively to these positions.

For the electrostatic contours of the topomer CoMFA-1 model relating to the fragment Ra and Rb is represented in Figure 6(b) and Figure 6(d) respectively. Figure 6(c) shows a blue color overlying methyl at position R1 with a fraction Ra, reflecting the importance of the electron donor group in this position for enhancing activity. For the Rb fragment, Figure 6(d) shows the appearance of large blue colored sector around carbon in position X. It is reported that this is a blue contour which did not appear as formed in the map. CoMFA model electrostatic contour.

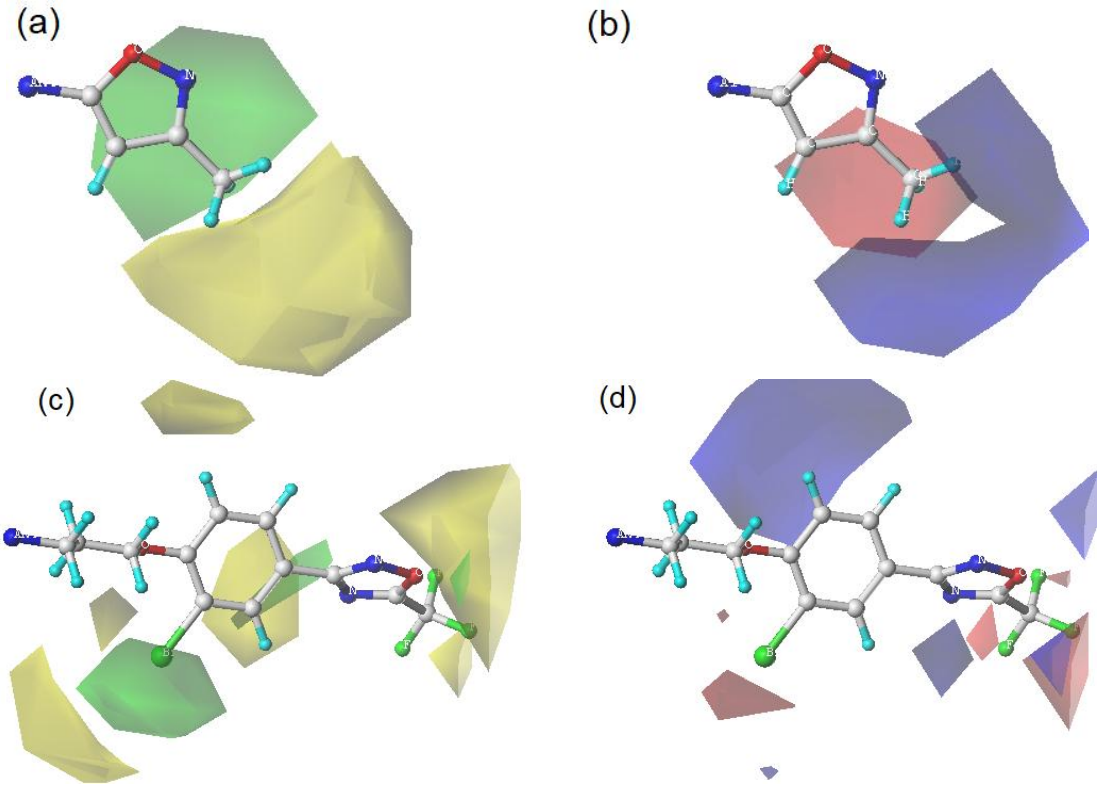

Figure 6. 3D contour of Topomer CoMFA-1 model for Ra and Rb of compound N°23: (a) Steric field map of Ra; (b) electrostatic field map of Ra; (c) steric field map of Rb ; (d) electrostatic field map of Rb.

3.6. Validation of QSAR model

Numerous studies show that good values of the parameters Q^2 and R^2 do not always imply that the models have good predictive capacities, for this the established QSAR models have been evaluated by external validation, using 8 compounds reserved test set which was not entered to build it from the model. statistical parameters were calculated and were used to confirm the stability and predictive capacity of the models. The results of the external validation parameters are listed in Table 6. In this work, the selected QSAR models gave the R^2_{ext} and r^2m values of 0.750 and 0.587 (HQSAR), 0.843 and 0.787 (CoMFA), 0.953 and 0.609; (CoMSIA) and 0.749 and 0.653 (CoMFA topomer) and steep regression lines with k and k' values of 0.823 and 1.129; (HQSAR), 0.972 and 1.00 (CoMFA), 0979 and 1.008 (CoMSIA), and 0.972 and 1.00 (CoMFA topomer) for pIC50 inhibitory activity respectively. Table 6 Based on the values of the performance criteria parameters of the QSAR models r_0^2, $r_0'^2$, $(R^2 - R^2_0) / R^2$, $(R^2 - R'^2_0) / R^2$, rm'^2, $\bar{r}^2m$, Δrm^2 and Δrm^2 in the data test (Table 6), it is obvious that all these parameters pass all the validation criteria with success. And therefore all models are reliable and could be powerful for new promoter compounds with high activity against CVB3. The graphs of Figure 7 represented with distribution of experimental and predicted values relative to the different QSAR models established

3.7. Molecular docking results

For a thorough understanding of the crucial interactions of the lesser and more potent inhibitors (compound N°23 and N°18), these compounds were anchored in the active site of the protein. In molecular docking studies, the 9 output conformations were classified according to the affinity score. according to the affinity values we have chosen the best poses. Figure 8 illustrates the nature of the best-pose interactions of Compound N°23 and Compound N°18 with the selected active site residues.

Table 6. ***External validation results of the four models developed***

Parameters	3D-QSAR			
	CoMFA	CoMSIA	Topomer CoMFA-1	HQSAR
r_0^2	0,848	0,823	0,765	0,796
$r_0'^2$	0,788	0,710	0,595	0,671
R^2	0,843	0,953	0,749	0,750
k	0,856	0,856	0,853	0,853
k'	1,104	1,121	1,143	1,129
$(r^2 - r^2_0) / r^2$	-0,005	0,137	-0,022	-0,062
$(r^2 - r'^2_0) / r^2$	0,066	0,255	0,206	0,104
r_m^2	0,787	0,609	0,653	0,587
$r_m'^2$	0,644	0,483	0,455	0,540
$\overline{r}^2_m$	0,715	0,546	0,554	0,564
Δr_m^2	-0,143	-0,126	-0,198	-0,048
Δr_0^2	0,060	0,113	0,170	0,125

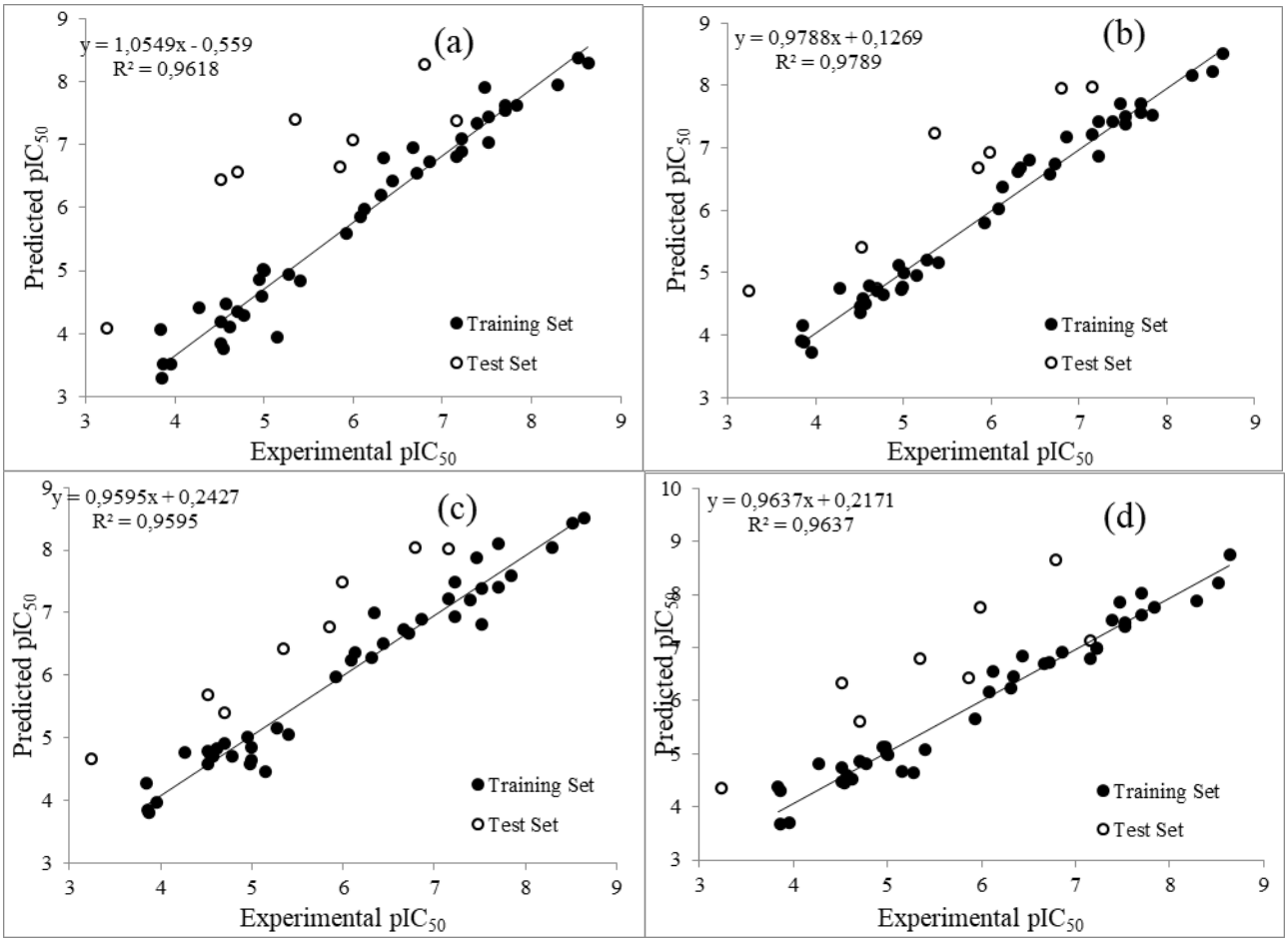

Figure 7. Relationship between experimental and predicted values for CoMFA topomer (a), CoMFA (b), CoMSIA (c), HQSAR (d) models.

The modes of interaction between the most active compound N°23 and the active site are shown in Figure 8, which shows two hydrogen bonds between the nitrogen atom of oxadiazole and the fluorine atom of R5 and amino acids Arg-143 and His-40 with distances of 2.47 Å and 2.89 Å, respectively. Thus the three fluorine atoms of the R4 group form halogen (fluorine) bonds with the amino acids Val-162 (3.28 Å) and Glu-71 (3.56 Å) Leu-127 (3.46 Å). However, a pi-donor hydrogen bond type bond was made between isoxazole oxygen and Gly-166 (2.67 Å). In addition, two pi-alkyl type interactions are observed between bromine and the nucleus or oxadiazole and the amino acids His-161 (4.68 Å) and Cys-147 (5.37 Å) respectively. These results provide evidence of the critical role of the amino acids Arg-143 and His-40 for the stability of the ligand in the active site.

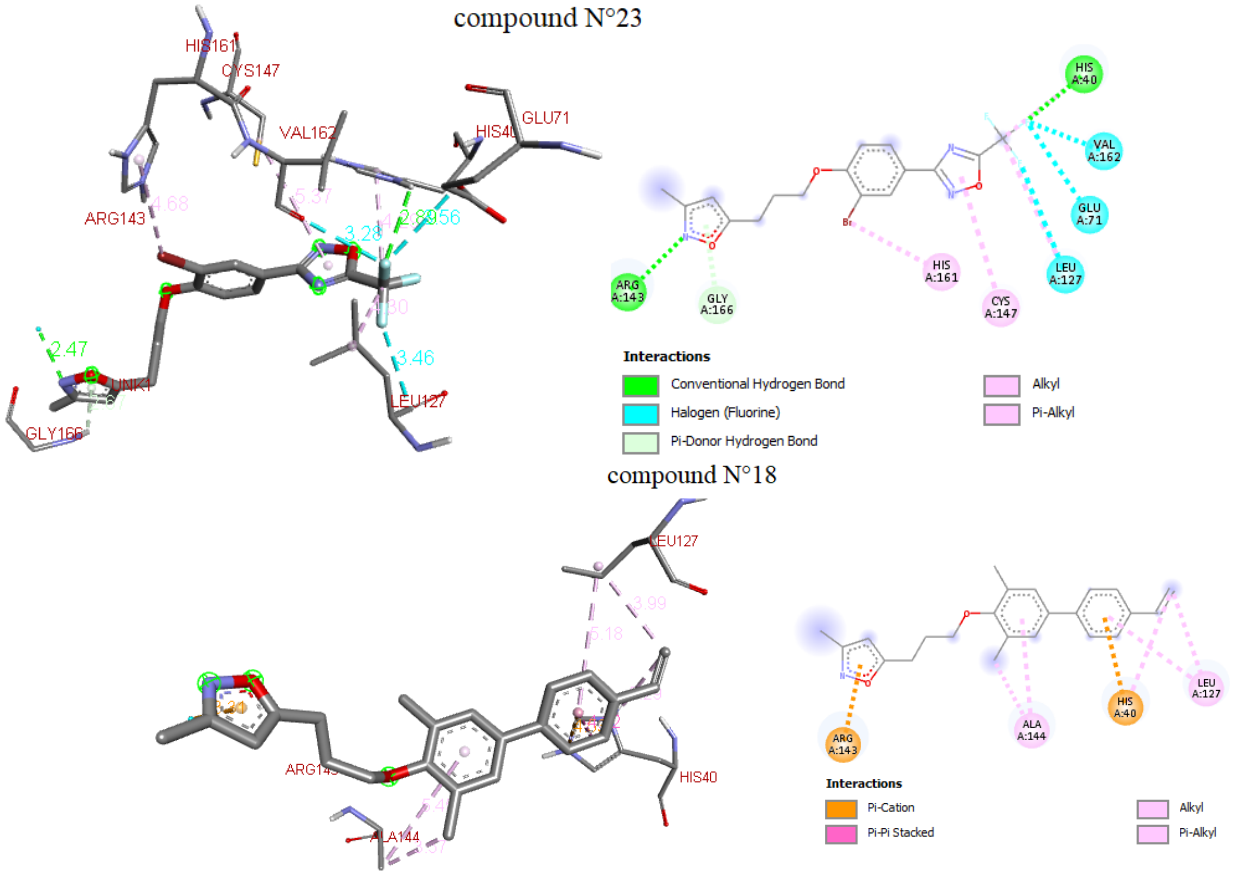

Figure 8. Binding modes and interactions of the most active (N°23) and least active (N°18) compound obtained from molecular docking.

However, compound 48 does not show any hydrogen-like bond. The isoxazole and phenyl rings at the R4 position form pi-cation bonds with the amino acids Arg-134 (3.31 Å) and His40 (4.53 Å) respectively. However, pi-alkyl-type interactions do form with the amino acids Ala-144 (3.57 Å) and Leu-127 (3.99 Å). The low activity of compound N°18 confirms the importance of the amino acids Arg134 and Lys65 with hydrogen bonding in the activity against CVB3. By comparing the molecular docking results with those obtained by 3D-QSAR analysis, it is corroborated that a surrogate with the hydrophobic characteristic promotes the Inhibition of activity against CVB3, a result compatible with the potential interaction with the Arg-134 residue by hydrogen-like interactions with the nitrogen atom doublet of diazfuran. 3D-QSAR results show that an electron-rich group can establish hydrogen bonds with His-40 and Arg-143 residues, interactions confirmed by docking simulations. In order to validate the ability of the molecular docking technique to predict ligand conformations in the active site of proteins, crystal breeding of the

G85 ligand and the superposition of the anchored ligand and the native crystal ligand were performed in Figure 9. The RMSD value is fair and less than 2 (1,708 Å).

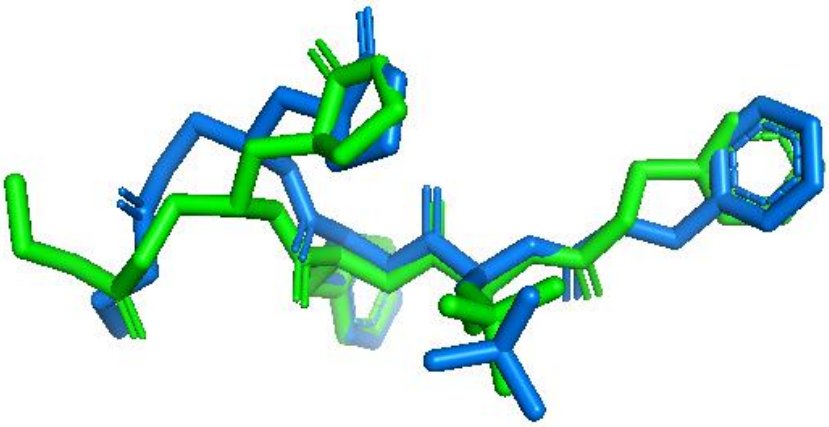

Figure 9. Re-docking pose with an RMSD value of 1,708 Å (blue = original, green = docked)

3.8. Design of new compounds

The developed 3D and 2D QSAR models and the study of molecular docking interactions provide guidelines for the design of new conduits with improved inhibitory activity. Using 3D-QSAR, we observed that steric and hydrophobic group and hydrogen bond acceptor play an important role in the activity of the study compounds. The substituents R2, and R2 and R3 have been modified, while the isoxazole ring and the phenyloxy propyl group have been retained as the basic structure. Larger groups with a more hydrophilic polar property than methyl were added at the R1 position. Steric and electron acceptor substituents have been introduced at the R5 position to the R3 group. Also steric groups at the R2 position. Using the information obtained from the 2D / 3D-QSAR molecular anchor, we propose four novel CVB3 virus inhibitors, which are optimized and aligned on the same template as the compounds in the dataset. The chemical structure and predicted activity values of the new compounds and the most potent inhibitor in the data set are shown in Table 7. Based on the models obtained, we proposed four molecules with high activity as inhibiting agents against the coxsackievirus B3 virus:A1 with inhibitory activities of pIC_{50} = 9.073 using model CoMFA, A2 with inhibitory activities of pIC_{50} = 8.990 using model CoMSIA, A3 with inhibitory activities of pIC_{50} = 8.840 using model HQSAR and A4 with inhibitory activities of pIC_{50} = 8.56 using the CoMFA topomer model. Molecular docking analysis was used to identify interactions of newly designed compounds with receptor (PDB ID: 3ZZD) using the same AutoDock 4.2.6 software. The molecular docking results of four proposed molecules are collected in Table 7.

All the compounds designed showed binding energy values between 7.2 and 7.4 kcal / mol, they have more affinity than the most active compound in the given base (N°23) 6.9 kcal / mol. The lowest binding energies and the best interactions were estimated to confirm and verify the best conformation of the designed ligands The analysis of the interactions and binding affinities of the four new compounds are shown in Figure 10. The best ligands are A3 and A4 which formed four hydrogen bonds, while ligand A2 and A1 formed three and two hydrogen bonds respectively. for the compound A3 the hydrogen bonds formed between the oxygen of phenyloxy and the residue His 40, between the oxygen of oxadiazole and the residue Gly-145 and between two fluorine atoms of the isoxazole group and the residues Gly-166 and Arg-143, these two fluorine atoms have also formed a halogen-type bond (fluorine) with Gly-164 and Thr-142. moreover the compound A3 shows a carbon hydrogen bond and two pi-donor hydrogen bond with Asn165 , Cys-147 and Glu-24 respectively, and pi-pi T - sheaped and pi alkyl with Phe-25 and Ala-144 respectively. for the compound A4 has formed four hydrogen bonds between two fluorine atoms of group R2 and the residues Arg-39 and His-40 and between two fluorine atoms of group R4 and the residues His-166 and Cys-147. thus all these fluorine atoms have formed halogen-type bonds (fluorine) with the residues Arg-143, Glu71, Val-62 and Leu-127.also pi-

cation and pi-alkyl bonds have been made between residus Lys42 and Phe25 respectively. The compound A1 exhibited two hydrogen bonds between the oxygen and the fluorine atoms of the isoxazole group R4 and the residues Glu-24 and Lys-108 respectively. even if this compound forms only two bonds of hydrogen type but it reveals a rather high affinity, we could justify this by the high number of interactions of pi alkyl and alkyl type, where two pi-alkyl bonds with the residues Phe-25 and Arg-143, and two alkyl bonds with Ala-144 and His-40. In addition a pi-sulfide type bond was made with residue Cys-147; For the compound A2, hydrogen bonds have formed between the oxygen and the nitrogen of isoxazole R4 and the residues Arg143 and Thr142 respectively, and between the oxygen of NO_2 of group R2 and the residue Cys147. Moreover a single pi-alkyl bond was made with the Leu127 residue. These interactions explain the stability and the strong activity of the proposed compound, especially hydrogen-type bonds because it is the shortest bond in all other bonds. We can report that the compound A2 realized three hydrogen bond but with weak affinity than A1 of only two bonds, because of the lack of other interactions in the compound A1 (a single bond type pi-alkyl).

Table 7. ***Structure, pIC_{50} predited and affinity values of newly designed compounds based on QSAR models***

Compounds	Structure	CoMFA	CoMSIA	CoMFA Topomer	HQSAR	Affinity(kcal/mol)
A149	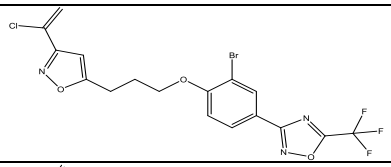	9,073	8,072	8.56	6,182	-7.4
A2 29	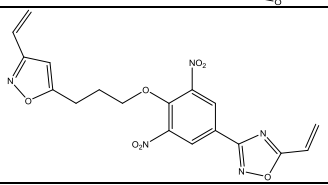	7.62	8,990	7.11	6,438	-7.2
A3O9	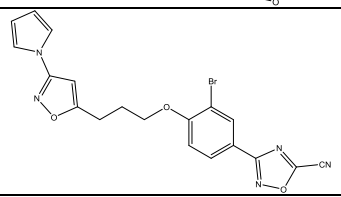	6,316	6,802	7.20	8,840	-7.4
A4 47	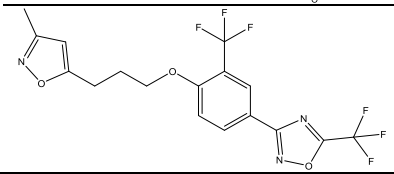	8,665	8.66	8.56	8,066	-7.4
Most active N°23		7,427	6,507	6.24	6,71	-6.9

3.9. Dynamic molecular simulation

Figure 11 represents the dynamic molecular simulation of the complex formed by compound A3 and the selected protein active site. The evolution of RMSD during the simulation time shows a variation between 1.6 and 1.4 starting from 10 ns, with significant stability.

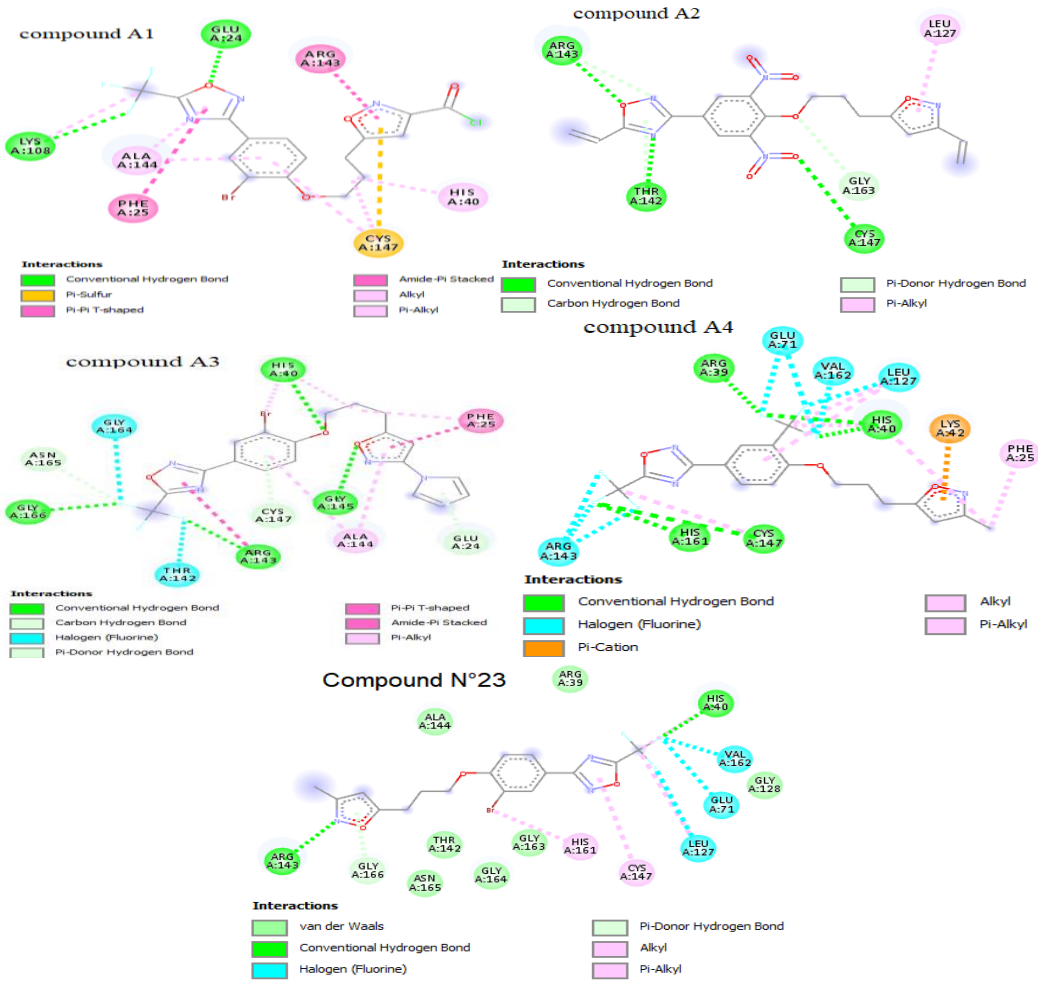

Figure 10. 2D docking poses showing interactions of new designed compounds A1, A2, A3 and A4.

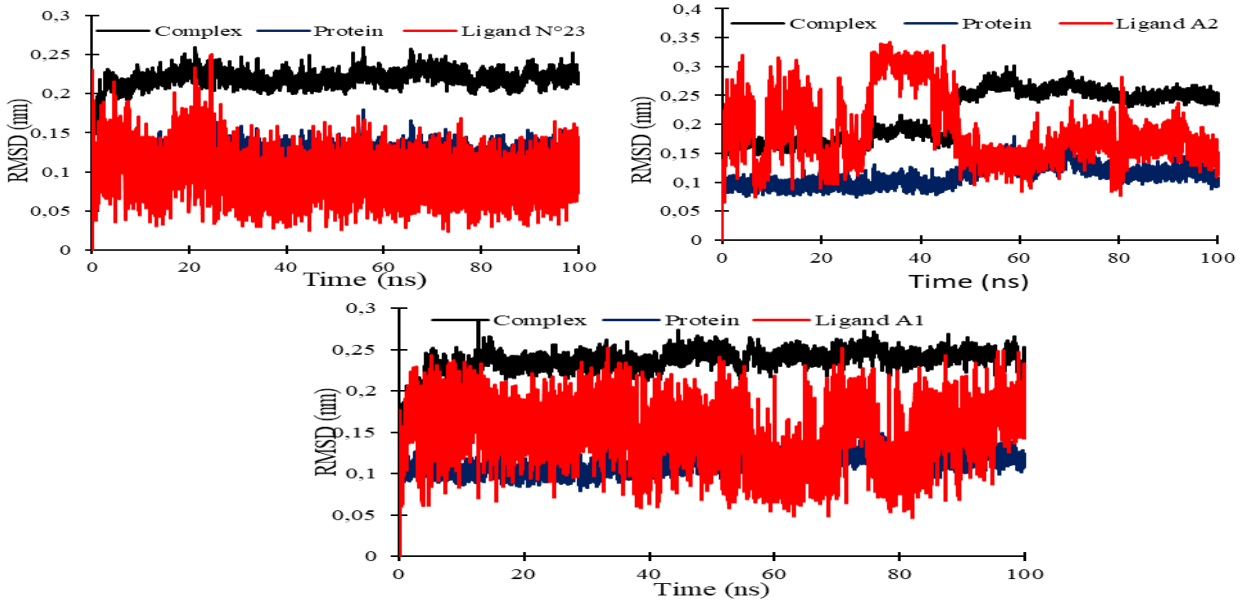

Figure 11. Root mean square deviation (RMSD) plots of backbone atoms of three selected systems.

The variation of the RMSF fluctuation values of the complex used also shows a weak evolution which indicates that the interactions of complex is less flexible in the active site. The flexibility of the protein structure was evaluated in terms of RMSF. RMSF calculations were performed for each protein residue. As shown in Figure 12, the A1 and A2

complexes show a weak fluctuation and do not exceed 0.2nm. In the case of complex N°23 also the fluctuations do not exceed 0.2 nm, except at residue 128 which shows a fluctuation of order of 0.23 nm. In addition, the stability of these complexes was also evaluated by monitoring the evolution of the radius of gyration (Rg). As shown in Figure 13, the calculated Rg values for the three complexes are stable throughout the simulation time. The number of hydrogen bonds made during the similation time is represented in Figure 14, as it is shown the complex A2 shows more of the hydrogen bonds.

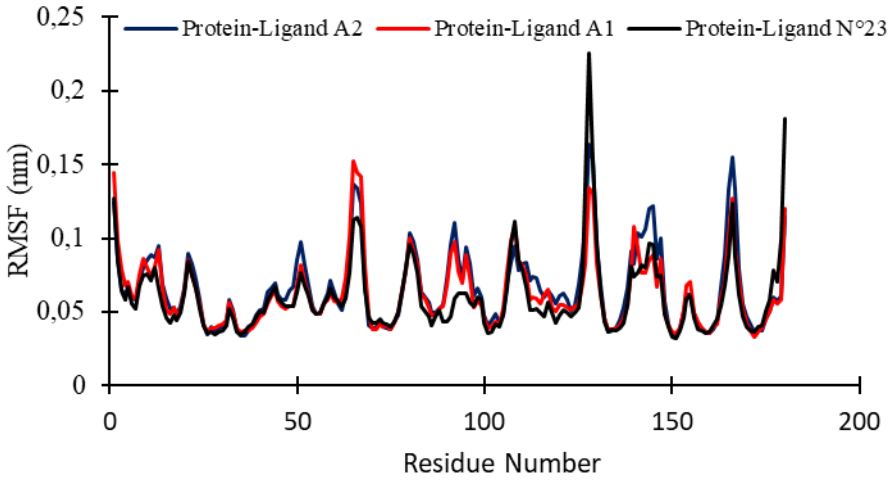

Figure 12. Root mean square fluctuation (RMSF) plots of backbone atoms of three selected systems.

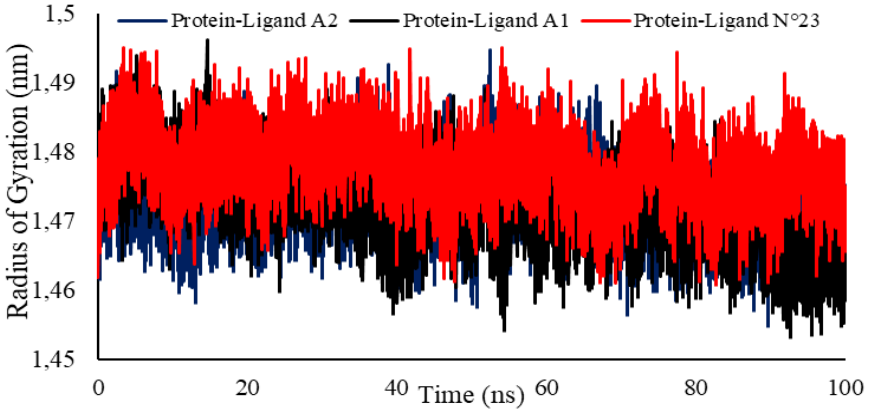

Figure 13. Radius of gyration (Rg) of three selected systems.

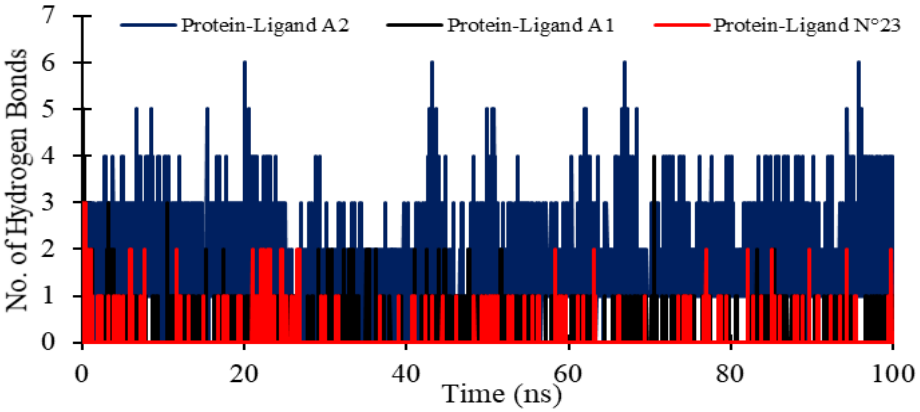

Figure.14 Number of hydrogene bons pf three systems selected during 100 ns.

3.10. Binding free energy simulation

The post dynamic MM-GBSA analysis of binding free energy (ΔG_{Bind}) calculation was calculated using gmx_MMPBSA tool using the equally spaced 100 frames from the last 90-100ns interval. The computed of binding free energy for the protein ligand complexes is depicted in Table 8.

Table 8. ***Binding free energy for protein-ligand complexes estimated using MM-GBSA analysais***

Energy Component	Compound A2		Compound A1		Compound N°23	
	Average	Std. Dev.	Average	Std. Dev.	Average	Std. Dev.
VDWAALS	-34,6237	3,1474	-45,5732	2,9206	-42,8803	3,5116
EEL	-2,4534	0,4267	-0,3886	0,1511	-0,9512	0,5307
EGB	3,0552	0,2833	1,4313	0,1533	2,1048	0,4955
ESurf	-4,5087	0,2597	-4,7929	0,2534	-3,7094	0,2898
ΔG gas	-37,077	3,1501	-45,9618	2,9191	-43,8315	3,7763
ΔG solv	-1,4535	0,3199	-3,3616	0,2238	-1,6046	0,5144
ΔG total	-38,5305	3,2111	-49,3234	3,0352	-45,4361	3,6505
ΔGbind	-25,6466	3,95	-40,6487	3,84	-31,5956	3,9908

From the results of the free energy calculations, it was noted that the van der Waals erergy made a major contribution to the total binding energy. The calculated average ΔG Bind of the complex A2, A1 and compouind N°23 in complex with the 3ZZD was found -25,6466 kcal / mol, -40,6487 and -31,5956 kcal/mol, respectively. A more negative value shows stronger binding, which is clearly shown in compound A01 newly designed by model CoMFA.

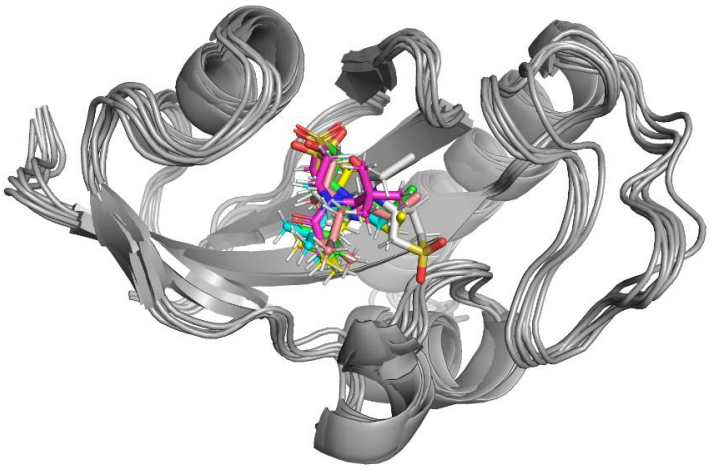

Figure 15. Superposition of three ligands selected in the binding site.

3.11. Lipinski's rule, bioavailability and ADME/Tox prediction of newly molecules.

Lipinski's rule, bioavailability and synthetic accessibility Newly designed molecules and the most potent inhibitor in the data set (N°23) were estimated using the online servers SwissADME and pkCSM. To ensure that the proposed candidates are viable drugs and having synthetic accessibility compared to the most active molecule N°23, we estimated certain pharmacokinetic properties (ADME/Tox) and certain physicochemical parameters of bioavailability Table 10. Lipinski's rule including five The physicochemical parameters: molecular weight (WM), number of the hydrogen bond donor (HBD), the number of hydrogen bond acceptors (HBA), the number of rotable bonds (NRB) and the LogP, the values obtained from these parameters have been collated in Table 9.

Table 9. ***Lipinski rule results of newly designed compounds***

N°	MW g/mol	HBA	HBD	LogP	TPSA	NBR	Bioavailability Score	Synthetic accessibility
	MW < 500	<10	<5	<5	< 140	< 10		
A1	480.62	7	0	4.9	91.25	7	0.55	3.15
A2	413.35	10	0	3.84	165.82	10	0.55	3.63
A3	440.26	7	0	4.16	102.90	7	0.55	3.32
A4	421.30	6	0	5.08	158.99	6	0.55	3.38
M23	432.19	9	0	4.83	74.18	7	0.55	3.15

The four designed compounds were within acceptable ranges in terms of water solubility and intestinal adsorption where they show a high intestinal absorption percentage of the oral drug (> 90%), indicating these drugs could have a possibility in oral formulation. The permeability of the newly synthesized compounds to the brain was estimated by calculating permeability of the blood brain barrier (BBB and CNS permeability), the four compounds were located at the values LogBB <-1 and Log PS <-3, which means that they are poorly distributed and difficult to move through the CNS. Therefore, all compounds were unlikely to cross the blood-brain barrier. Drug metabolism has been estimated by cytochrome P450, in particular CYPs (1A2, 2C9 / 19, 2D6 and 3A4) being responsible for the biotransformation of more than 90% of drugs undergoing phase I metabolism. All of the newly designed compounds have been shown to be the inhibitor of CYP1A2, CYP 2C9/2C19, and for CYP3A4 compounds A2, A3 and A4 are just inhibitors and substrates of CYP3A4. The toxicity evaluation of the compounds was carried out by prediction of the AMES test and Maximum Tolerate dose (Human), the results obtained indicate that all the candidates A1, A2, A3, and A4 apparently have no potential toxicity.

Table 10. ***ADMET results predicted in silico of newly designed compounds***

	Absorption			Distribution		Metabolism							Excretion		Toxicity	
						substrate		Inhibitor								
						CYP										
N°	Water solubility (log mol/L)	Caco2 permeability (%Absorbed	Intestinal absorption (human)	BBB permeability (Log BB)	CNS permeability (Log PS)	2D6	3A4	1A2	2C19	2C9	2D6	3A4	Total Clearance (Log ml/min/kg)	AMES toxicity	Max. tolerated dose (human)	
A1	-4.293	1.302	91.973	-1.577	-3	N	Y	Yes	Yes	Yes	No		No	0.089	No	0.503
A2	-5.688	-0.191	92.309	-1.864	-2.878	N	Y	Yes	Yes	Yes	No		Yes	0,476	Yes	-0.073
A3	-3.707	1.237	100	-1.34	-2.491	N	Y	Yes	Yes	Yes	No		Yes	-0.096	Yes	-0.551
A4	-5.355	1.264	90.718	-1.612	-2.209	N	Y	Yes	Yes	Yes	No		Yes	0.069	No	-0.143
M23	-5.278	0.666	93.056	-1.363	-2.9	**N**	**Y**	Yes	Yes	Yes	No		No	0.031	No	-0.049

Conclusion

In this study, the inhibitory activities of 49 inhibitors against CVB3 virus were used to develop predictive models for HQSAR, CoMFA, CoMFA topomer and CoMSIA. The models chosen provided significant statistical indicators with values of R^2 and Q^2 and R^2_{ext} are 0.953, 0.980, 0.977 and 0.962; 0.819, 0.83, 0.748 and 0.804 and 0.750, 0.749, 0.843 and 0.953, for the HQSAR CoMFA topomer, CoMFA, CoMSIA models.

From the results of the models obtained four molecules were predicted with a higher activity A1, A2, A3, and A4. Moreover, molecular docking and molecular dynamics simulation studies were performed to justify the validation of

established models and to understand the mechanism of ligand-receptor interaction. The molecular docking results show that the four predicted molecules exhibit a very high binding energy in the binding site, in particular molecules A1 and A4. The compound A1, A2 and the most active of the data set subjected to a dynamic study to evaluate the stability of the protein ligand complex in terms of RMSD, RMSF, Rg and hydrogen bond number, the results obtained display the stability of the complex during the simlation trajectory. The free energy calculation by MM-GBSA justifies the stability of the selected system and confirms the molecular docking result. The reliability of the molecules predicted as drugs was estimated by the ADMET study which revealed good results in molecules A1 and A3 in particular. This work has provided a structural information base that explains the activity of the phenyloxy propyl oxazole derivative as well and reliable for the design of a novel inhibitor against CVB3 virus.

References

[1] M. Tebruegge et N. Curtis, " Enterovirus infections in neonates ", in *Semin. Fetal Neonatal Med.* 14(4) (2009) 222-227.

[2] L. van der Linden, K. C. Wolthers, et F. J. Van Kuppeveld, " Replication and inhibitors of enteroviruses and parechoviruses ", *Viruses*, 7(8) (2015) 4529-4562.

[3] M. Šála *et al.*, « SAR studies of 9-norbornylpurines as Coxsackievirus B3 inhibitors ", *Bioorganic Med. Chem. Lett*, 21(14) (2011) 4271 −4275.

[4] N. Khetsuriani, E. S. Quiroz, R. C. Holman, et L. J. Anderson, " Viral meningitis-associated hospitalizations in the United States, 1988–1999 ", *Neuroepidemiology*, 22(6) (2003) 345-352.

[5] M. Šála *et al.*, " SAR studies of 9-norbornylpurines as Coxsackievirus B3 inhibitors ", *Bioorganic Med. Chem. Lett*, 21(14) (2011) 4271-4275.

[6] D. L. Barnard, " Current status of anti-picornavirus therapies ", *Curr. Pharm. Des*, 12(11) (2006) 1379-1390.

[7] A. M. De Palma, I. Vliegen, E. De Clercq, et J. Neyts, " Selective inhibitors of picornavirus replication ", *Med. Res. Rev*, 28(6) (2008) 823-884.

[8] S. E. Adeniji, S. Uba, et A. Uzairu, " Computational investigation and molecular docking simulation of some bioactive compounds as potent inhibitors against tuberculosis receptor ", *Mor. J. Chem*, 7(4) (2019) 697-714.

[9] F. Z. E. Chokrafi, F. Khalil, et M. Bouachrine, " QSAR studies antiproliferative activity of heterocyclic compounds based on 2-cyano-N-(3-cyano-4, 5, 6, 7-tetrahydrobenzo [b] thiophen-2-yl). ", *Mor. J. Chem*, 5(4) (2017) 590-599.

[10] B. Elidrissi *et al.*, " The acute toxicity of nitrobenzenes to Tetrahymena pyriformis: Combining DFT and QSAR studies ", *Mor. J. Chem* , 3(4) (2015) 848-860.

[11] N. Aoumeur, S. Belaidi, N. Tchouar, M. Ouassaf, T. Lanez, et S. Chtita, " Molecular docking studies for the identifications of novel antimicrobial compounds targeting of staphylococcus aureus ", *Mor. J. Chem*, 9(2) (2021) 274-289.

[12] H. Hajji *et al.*, " In Silico Investigation on the Beneficial Effects of Medicinal Plants on Diabetes and Obesity: Molecular Docking, Molecular Dynamic Simulations, and ADMET Studies ", (2021).

[13] K. Tabti *et al.*, " In silico design of novel PIN1 inhibitors by combined of 3D-QSAR, molecular docking, molecular dynamic simulation and ADMET studies ", *J. Mol. Struct.*, 1253 (2022) 132291.

[14] V. A. Makarov, O. B. Riabova, V. G. Granik, P. Wutzler, et M. Schmidtke, " Novel [(biphenyloxy) propyl] isoxazole derivatives for inhibition of human rhinovirus 2 and coxsackievirus B3 replication ", *J. Antimicrob. Chemother.*, 55(4) (2005) 483-488.

[15] M. Schmidtke, P. Wutzler, R. Zieger, O. B. Riabova, et V. A. Makarov, " New pleconaril and [(biphenyloxy) propyl] isoxazole derivatives with substitutions in the central ring exhibit antiviral activity against pleconaril-resistant coxsackievirus B3 ", *Antivir. Res.*, 81(1) (2009) 56-63.
[16] E. Muratov *et al.*, " HiT QSAR analysis of anti-coxsackievirus b3 activity of [(biphenyloxy) propyl] isoxazole derivatives ", *Antivir. Res.*, 2(78) (2008) A60-A61.
[17] A. Egorova, E. Kazakova, B. Jahn, S. Ekins, V. Makarov, et M. Schmidtke, " Novel pleconaril derivatives: Influence of substituents in the isoxazole and phenyl rings on the antiviral activity against enteroviruses ", *Eur. J. Med. Chem.*, 188(2020) 112007.
[18] W. Yan, G. Lin, R. Zhang, Z. Liang, et W. Wu, " Studies on the bioactivities and molecular mechanism of antioxidant peptides by 3D-QSAR, in vitro evaluation and molecular dynamic simulations ", *Food Funct.*, 11(4) (2020) 3043-3052.
[19] H. HAJJI, " Antiproliferative Activity: Discovery of new Benzoxanthenes derivatives by Using Various Statistical Methods 2D/3D-QSAR and Molecular Docking ", *RHAZES: Green and Applied Chemistry*, 12 (2021) 40-59.
[20] K. Tabti *et al.*, " Computational investigation of pyrrolidin derivatives as novel GPX4/MDM2–p53 inhibitors using 2D/3D-QSAR, ADME/toxicity, molecular docking, molecular dynamics simulations, and MM-GBSA free energy ", *Struct. Chem.*, 33(4) (2022) 1019-1039.
[21] K. TABTI, A. Sbai, H. Maghat, M. Bouachrine, et T. Lakhlifi, " 2D and 3D-QSAR/CoMSIA Comparative Study On a Series of Thiazole Derivatives as SDHI Inhibitors ", *Maghreb. J. Pure & Appl. Sci.*, 6(2) (2020).
[22] L. El Mchichi *et al.*, " In silico design of novel Pyrazole derivatives containing thiourea skeleton as anti-cancer agents using: 3D QSAR, Drug-Likeness studies, ADMET prediction and molecular docking ", *Mater. Today: Proc.*, (2021).
[23] K. Tabti, L. Elmchichi, A. Sbai, H. Maghat, et T. Lakhlifi, " HQSAR, CoMFA, CoMSIA docking studies and simulation MD on quinazolines/quinolones derivatives for DENV virus inhibitory activity ", (2022).
[24] C. L. Waller, " A comparative QSAR study using CoMFA, HQSAR, and FRED/SKEYS paradigms for estrogen receptor binding affinities of structurally diverse compounds ", *J Chem Inf Comput Sci.*, 44(2) (2004) 758-765.
[25] R. Abdizadeh, F. Hadizadeh, et T. Abdizadeh, " QSAR analysis of coumarin-based benzamides as histone deacetylase inhibitors using CoMFA, CoMSIA and HQSAR methods ", *J. Mol. Struct.*, 1199 (2020) 126961.
[26] Z. Ke *et al.*, " 3D-QSAR and molecular fragment replacement study on diaminopyrimidine and pyrrolotriazine ALK inhibitors ", *J. Mol. Struct.*, 1067(2014) 127-137.
[27] A. O. Ajala et C. O. Okoro, " 3D-QSAR Topomer CoMFA Studies on 10 N-Substituted Acridone Derivatives ", (2012).
[28] K. TABTI, "QSAR Studies of New Compounds Based on Thiazole Derivatives as PIN1 Inhibitors via statistical methods ", *RHAZES: Green and Applied Chemistry*, 9 (2020) 70-91.
[29] P. K. Balasubramanian, A. Balupuri, C. G. Gadhe, et S. J. Cho, " 3D QSAR modeling study on 7-aminofuro [2, 3-c] pyridine derivatives as TAK1 inhibitors using CoMFA and COMSIA ", *Med. Chem. Res.*, 24(6) (2015) 2347-2365.
[30] A. Golbraikh et A. Tropsha, " Beware of q2! ", *J. Mol. Graph. Model.*, vol. 20, n° 4, p. 269-276, 2002.
[31] K. Roy, " On some aspects of validation of predictive quantitative structure–activity relationship models ", *Expert Opin. Drug Discov.*, 2(12) (2007) 1567-1577.
[32] K. K. Roy, A. Dixit, et A. K. Saxena, " An investigation of structurally diverse carbamates for acetylcholinesterase (AChE) inhibition using 3D-QSAR analysis ", *J. Mol. Graph. Model.*, 27(2) (2008) 197-208.

[33] S. Sridhar, A. Hahn, et M. Govindarasu, " Cyber–physical system security for the electric power grid ", *Proc. IEEE*, 100(1) (2011) 210-224.
[34] N. N. Mrabti, " QSAR study and molecular docking of benzimidazole derivatives inhibitors of p38 kinase ", *Mor. J. Chem*, 6(3) (2018) 511-524.
[35] A. El Hadki *et al.*, " DFT and Molecular docking study of natural molecules proposed for COVID-19 treatment ", *Mor. J. Chem*, vol. 9(2) (2021) 198-209.
[36] M. S. V. Tresanco, M. E. V. Tresanco, P. A. Valiente, et E. M. Frías, " gmx_MMPBSA (Version v1. 4.2) ", *Zenodo.[(accessed on 18 June 2021)]*, (2021).
[37] B. R. Miller III, T. D. McGee Jr, J. M. Swails, N. Homeyer, H. Gohlke, et A. E. Roitberg, " MMPBSA. py: an efficient program for end-state free energy calculations ", *J. Chem. Theory Comput.*, 8(9) (2012) 3314-3321.

(2022) ; https://revues.imist.ma/index.php/morjchem